

Electronic Supplementary Information

Evolution of the active species of homogeneous Ru-based hydrogenation catalysts in ionic liquids

K. Janssens,^a A. L. Bugaev,^b E. G. Kozyr,^{b,c} V. Lemmens,^a A. A. Guda,^b O. Usoltsev,^b S. Smolders,^a A. V. Soldatov^b and D. E. De Vos^{a*}

^aCentre for Membrane Separations, Adsorption, Catalysis and Spectroscopy for Sustainable Solutions (cMACS), Department of Microbial and Molecular Systems (M2S); KU Leuven, Celestijnenlaan 200F, post box 2454, 3001 Leuven (Belgium).

^bThe Smart Materials Research Institute, Southern Federal University, Sladkova 178/24, 344090 Rostov-on-Don, Russia

^cDepartment of Chemistry, University of Turin, Via Giuria 5, 10125 Turin, Italy

Chemicals

Tetrabutylphosphonium bromide (Sigma-Aldrich, 98%), Acetone (Acros, 99%), *n*-dodecane (J&K, 95%), *n*-tetradecane (TCI, 99%), N₂ (Air Liquide, α1), H₂ (Air Liquide, N40), CO (Air Liquide, N37), propene (Air Liquide, N25), HBr (Sigma-Aldrich, 48% in water), ruthenium(III) bromide hydrate (Alfa, Ru 25% min), tricarbonyldichlororuthenium(II) dimer (Sigma Aldrich), *N,O*-bis(trimethylsilyl)trifluoroacetamide (Sigma-Aldrich, BSTFA + TCMS 99:1), potassium bromide (Acros, 99%), benzene (Carl Roth 99%), chloroform (Fisher, 99%), hexane (Acros, 97%) and Br₂ (Sigma-Aldrich, +99.5%). All chemicals were used as received.

Product analysis

After reaction a spontaneous phase separation occurs between the IL and the dodecane layer.^{1,2} A liquid aliquot of the dodecane layer was taken for GC analysis, performed on a Shimadzu GC-2013 instrument equipped with a DB-FFAP column. GC analysis of the silylated polar intermediates (isopropanol) was performed on a Shimadzu GC-2010 instrument equipped with a CP SIL-5 CB column. The quantification was performed by comparison of the peak areas in GC with the peak area of the internal standard. For all products, a calibration curve was obtained by extracting different amounts of the product together with a constant amount of the internal standard to the dodecane layer. In the case of isopropanol, a calibration curve was made for the combined derivatization and extraction.

However, at high conversions and propene selectivities, the amount of propane is very low compared to propene. Therefore, to maintain high accuracy on the exact propene/propane selectivity, in addition to quantitative GC analysis, we performed an independent analysis to determine the propene vs propane selectivity. Fourier Transformed Infrared (FT-IR) spectroscopy was performed on the gas in the headspace of the reactor, injecting a gas sample into a N₂ flow on a Gasmeter DX 4000 FT-IR gas analyzer. Spectra were processed using Calcmet standard software (v. 12.161), and corresponded well with the liquid phase composition. The use of FT-IR relies on a difference in vibrations of the =C-H alkene stretch (above 3000 cm⁻¹) compared to the -C-H alkane stretch (2800-3000 cm⁻¹). The Calcmet software allows for the accurate calculation of the propene vs. propene+propane ratio, thus indicating the selectivity of the system even at very low concentrations (below 1% of the formed C₃-compounds is present in the gaseous phase).

Apart from propene/propane and CO, no additional gaseous compounds were detected, indicating that no fragmentation of C₃ to C₂ products occurs (also confirmed with GC-MS). In the first liquid extraction, only propene, propane acetone and mono-bromopropanes were detected. In the extraction after a derivatisation reaction, only 2-propanol was observed. Both in literature^{1,2} and this work, no hydroformylation reactions are observed in the formation of C₄ products.

Boundary conditions

Based on previous literature reports on the hydrodeoxygenation of polyols to olefins, the applied reaction conditions are necessary to obtain high hydrogenation selectivity in combination with fast alcohol dehydration.^{1,2} Since the present study aims at elucidating the mechanism and potential routes for activation and deactivation, we did not re-optimize the conditions specifically for the hydrogenation of the model compounds (acetone/propene). Instead, we verified the key steps under the conditions that are most relevant for eventual application of this chemistry. Both the pretreatment step and the catalytic tests on the model substrates were performed under conditions optimized for the deoxygenation of waste glycerol, as this will be the most relevant application.¹ The suitable CO pressure range is 1-5 bar CO, with 1 bar CO corresponding to approximately 50mmol CO/mmol Ru for 2 mol% Ru_{cat}.¹ The hydrogen pressure was found to be optimal at 40 bar, but sufficient activity was observed in the 15-50 bar range.² The temperature is actually most decisive for the rate of dehydration of the (bio-)alcohols; the temperature was found to have only limited influence on the hydrogenation selectivity in the range from 180-220°C.^{1,2} The exact conditions applied in this study are described in the main manuscript under “Catalytic reaction”.

XAS analysis

Ex situ XAS data reported in Tables S1-S2 and Figures 1-6 of the main text were measured in the transmission mode resulting in the edge jump values of 0.8 – 1.4 for initial compounds and ca. 0.2 for those dissolved in IL. All *ex situ* spectra were analyzed in the Demeter package.³ Energy calibration using reference ruthenium foil measured simultaneously with the samples, normalization, background subtraction, extraction of $\chi(k)$ functions for EXAFS analysis and LCF of XANES (Figure 5 of the main text) were performed in the Athena program. Next, the fitting of the EXAFS data was performed in the Artemis program using $k^{1,2,3}$ -weighed data in the k -range from 4 to 15 Å⁻¹. The fitting was performed in real space, in the R -range from 1.0 to 3.0 Å. The number of independent points, $N_{idp} = 2\Delta k\Delta R/\pi \sim 14$. Theoretical amplitudes and phases were calculated by FEFF6 code² using crystalline structures of RuX₃ (X = Cl, Br), metallic *fcc* ruthenium, and cluster models of Ru₃(CO)₁₂ and [RuX₂(CO)₃]₂ complexes obtained from DFT. For every type of contribution interatomic distances (R), Debye-Waller parameters (σ^2), and coordination numbers (N) were set as independent variable parameters. Zero potential correction (ΔE_0) was considered as a common variable for all contributions. The amplitude reduction factor S_0^2 was fixed to 0.9.

Table S1. Structural parameters obtained from Fourier-analysis of EXAFS data for crystalline RuX₃ salts and those dissolved in IL.

	RuBr ₃	RuCl ₃	RuBr ₃ in IL	RuCl ₃ in IL****
$R_{\text{Ru-Br}}$ (Å)*	2.49	-	2.50	2.51
$N_{\text{Ru-Br}}$	6	-	4.3 ± 0.3	(3.7 ± 0.8)
$\sigma^2_{\text{Ru-Br}}$ (Å ²)**	0.004	-	0.005	0.003
$R_{\text{Ru-Cl}}$ (Å)*	-	2.35	-	2.40
$N_{\text{Ru-Cl}}$	-	6	-	(2.8 ± 0.4)
$\sigma^2_{\text{Ru-Cl}}$ (Å ²)**	-	0.005	-	0.003
$R_{\text{Ru-O}}$ (Å)***	-	1.80	-	-
$N_{\text{Ru-O}}$	-	0.8 ± 0.2	-	-
$\sigma^2_{\text{Ru-O}}$ (Å ²)	-	0.001	-	-

*the typical error in determination of interatomic distances was within 0.01 Å

**the typical error in determination of Debye-Waller parameters was within 0.001 Å²

***Ru–O contribution is related to water molecules present in the hydrated salt. Since the initial salts were present in hydrated state, Ru–O contribution was included to account for the presence of water in RuCl₃ sample, while in RuBr₃ it was neglected due to much weaker photoelectron backscattering amplitude of O compared to Br.

**** Due to the partial antiphase of Ru–Br and Ru–Cl signals their CNs correlate, and their absolute values should be treated with care.

Table S2. Structural parameters obtained from Fourier-analysis of EXAFS data for reference $[\text{RuBr}_2(\text{CO})_3]_2$ and $[\text{RuX}_2(\text{CO})_3]_2$ precursors dissolved in IL.

	$[\text{RuBr}_2(\text{CO})_3]_2$	$[\text{RuBr}_2(\text{CO})_3]_2$ in IL	$[\text{RuCl}_2(\text{CO})_3]_2$ in IL
N_{CO}	3.4 ± 0.2	2.2 ± 0.3	2.3 ± 0.3
$N_{\text{Ru-Br}}^*$	2.6	3.8	3.7
$R_{\text{Ru-Br}} (\text{\AA})^{**}$	2.55	2.56	2.55
$R_{\text{Ru-C}} (\text{\AA})$	1.91	1.84	1.86
$R_{\text{Ru-O}} (\text{\AA})$	3.06	3.00	3.02
$\sigma^2_{\text{Ru-Br}} (\text{\AA}^2)^{***}$	0.004	0.005	0.005
$\sigma^2_{\text{Ru-C}} (\text{\AA}^2)$	0.004	0.003	0.002
$\sigma^2_{\text{Ru-O}} (\text{\AA}^2)$	0.004	0.005	0.003

*defined as $6 - N_{\text{Ru-CO}}$

**the errors in determination of interatomic distances were within 0.01 \AA

***the errors in determination of Debye-Waller parameters were within 0.001 \AA^2

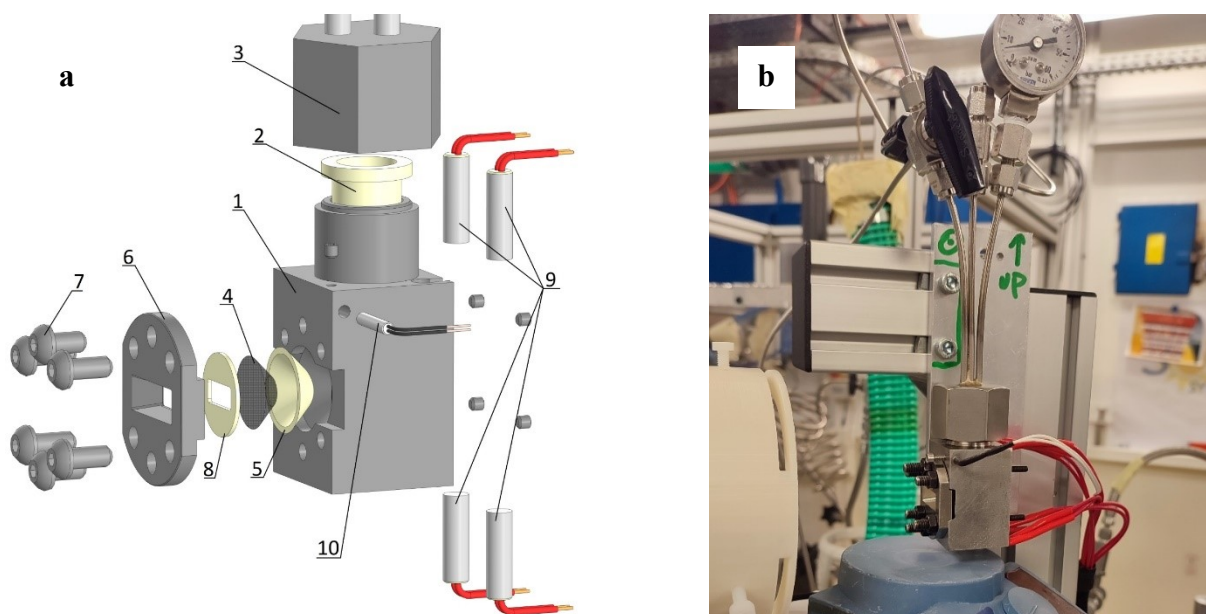


Figure S1. (a) Schematic drawing of the *in situ* stainless steel high-pressure cell (1) for fluorescence XAS measurements with a Teflon liner (2), a cap (3) with three Swagelok connections, a glassy carbon window (4) which is fixed to the open side of the cell with two Teflon/aluminum spacers (5 and 8) via the stainless steel overlay (6) attached to the cell body by six bolts (7). The cell was heated via four thermistors (9), the temperature being controlled by a thermocouple (10). (b) A photo of the cell during the measurements at SAMBA beamline of Soleil synchrotron.

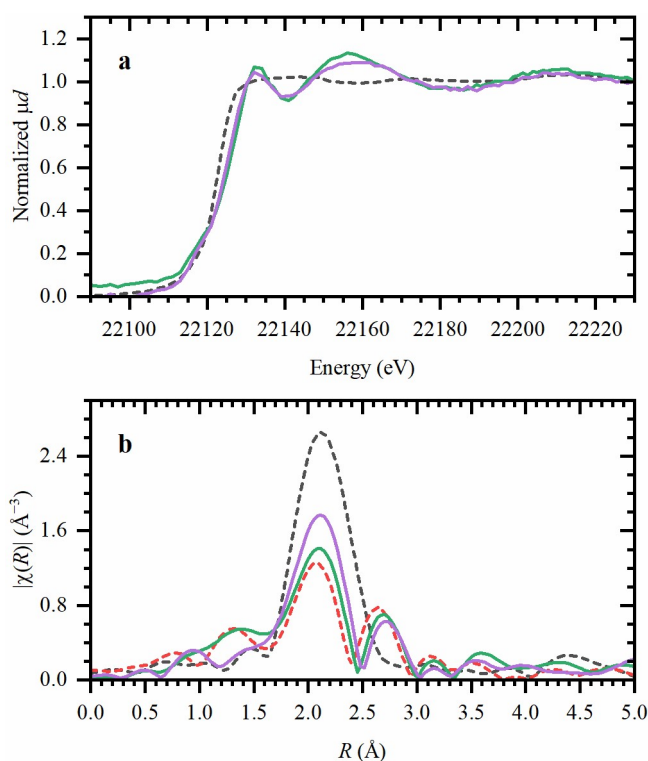


Figure S2. XANES (a) and phase-uncorrected FT-EXAFS (b) data for the reference RuBr_3 salt (dashed black) and $[\text{RuBr}_2(\text{CO})_3]_2$ compound before (dashed red), and catalytic species obtained from RuBr_3 salt dissolved in Bu_4PBr in presence of CO gas (solid green) and formaldehyde (solid purple).

In situ data were collected in the fluorescence mode for catalytic systems with low Ru-concentration under relevant conditions, which naturally resulted in worse signal-to-noise ratio. The overview of the collected data is shown in Figure S3. The following procedure was applied for the data analysis. As a the first step, a set of statistical criteria were calculated for the dataset using PyFitIt code.³⁻⁴ The first of the used criteria is a Scree plot (Figure S4a), which shows in the logarithmic scale the eigenvalues of the principal components. A common procedure to determine the number of significant component (i.e. those relevant to the real changes in the spectra and not noise) is to find an “elbow” point in this graph. Thus, 2 or 3 components should be used for this dataset. Since the Scree plot itself, as any other criterion, may not give an unambiguous estimation of the number of components, an additional criterion, viz. the Malinowski IND function, was considered (Figure S4b). The minimum of this function, which was found at $N = 3$, corresponds to the number of independent components. As a next step, the MCR-ALS, implemented in the MATLAB code,⁵⁻⁷ was applied to obtain not just abstract PCA components, but the components whose shape is relevant to the spectra of chemically independent species. This approach tries to decompose the whole spectral dataset, represented by a matrix \mathbf{D} of size $m \times n$, where m is the number of spectra in the dataset and n is the number of energy points, as $\mathbf{D} = \mathbf{CS}^T + \mathbf{E}$, where \mathbf{C} with size $m \times k$ are the concentration profiles of k pure components from matrix $\mathbf{S}(n \times k)$, and $\mathbf{E}(m \times n)$ is the error matrix. The resulting spectra and the concentration profiles of the corresponding species are shown in Figure 7a,b of the main text. Due to the noise and experimental artifacts in the spectra, the region for PCA and MCR-ALS analysis was limited to 22112-22220 eV as shown in Figure S3.

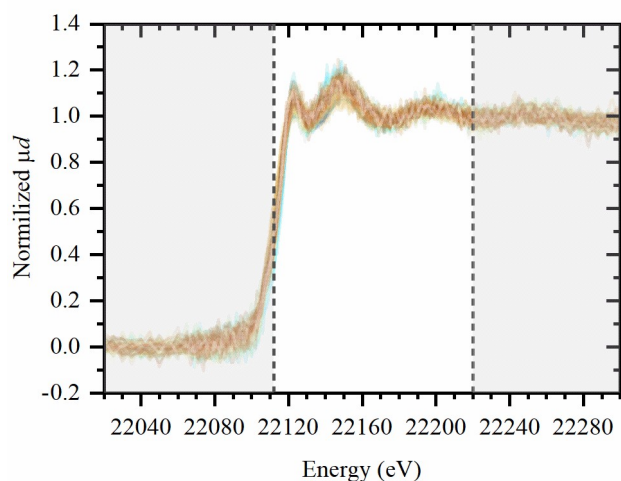


Figure S3. An overview of the *in situ* Ru *K*-edge data, with the region selected for PCA and MCR-ALS analysis highlighted by dashed vertical lines and white background.

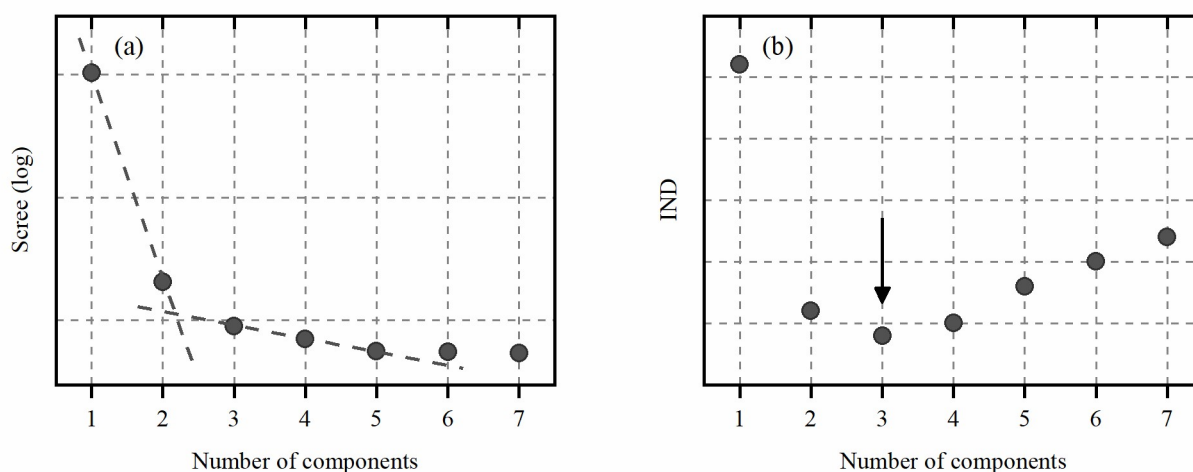


Figure S4. Scree plot (a) on IND function (b) for the dataset shown in Figure S3. The optimal number of components is determined according to the “elbow” in the Scree plot, or as a minimum of the IDN function.

DFT calculations

All calculations were performed using the ADF engine of AMS software⁸ at DFT level of theory with BLYP-D3 exchange-correlation potential⁹⁻¹¹ and TZP Slater-type basis set.¹² The choice of the potential and basis set was made based on the comparison of the Ru–ligand C, Ru–Cl and C–O distances in the relaxed structure with those obtained from EXAFS for $[\text{RuCl}_2(\text{CO})_3]_2$. The scalar relativistic effects were included within the Zero Order Regular Approximated (ZORA) Hamiltonian.¹³ Various possible geometries of the intermediate states were screened and those with lowest bond energy (the property calculated by ADF) were selected. For the optimized geometries, frequency analysis was performed confirming no negative frequencies for intermediate states and one negative frequency for the transition states. The relative energies shown in Figure 7 of the main text and Figures S5-S6, were calculated as the difference between final and initial structures. In case the final and initial structure contain different substrate and/or ligands, the necessary terms were added using the values obtained for isolated molecules (CO, H₂, HBr, acetone, 2-propanol, propene, propane). For the case, when the two Ru-sites were involved (Figure S3, in grey) the difference in energy were normalizer per one site (i.e. divided by 2).

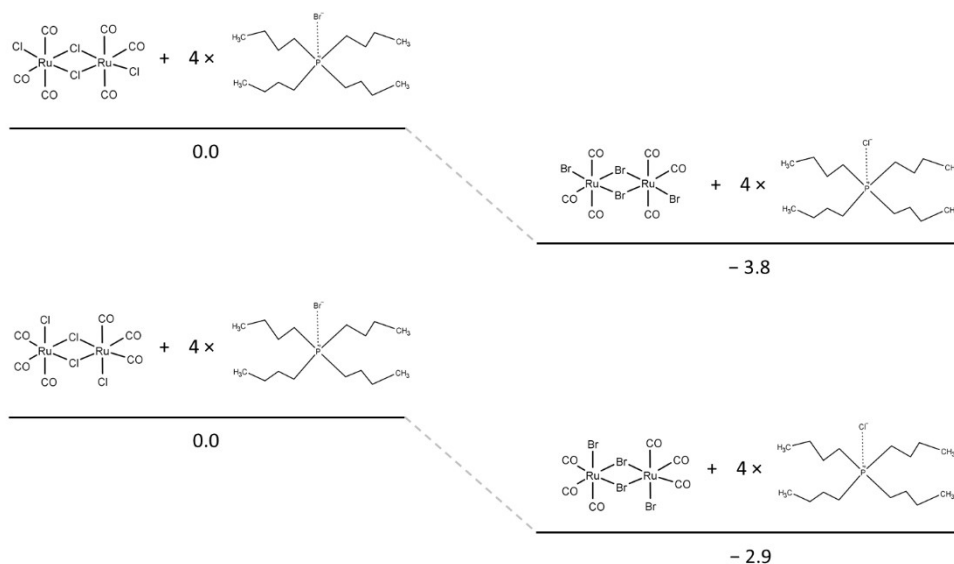


Figure S5. Relative energy change for the $\text{Cl}^- \leftrightarrow \text{Br}^-$ between in Br-rich IL and $[\text{RuCl}_2(\text{CO})_3]_2$ complex, calculated by DFT.

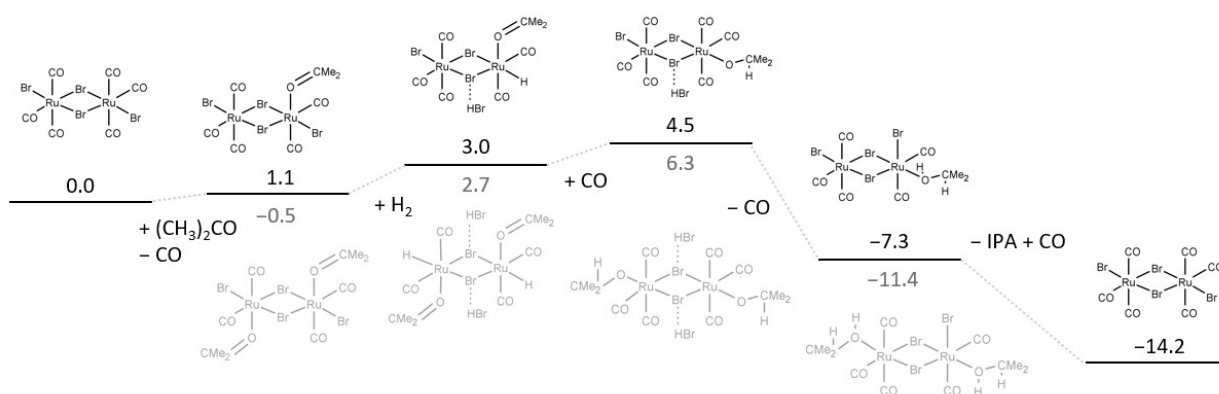


Figure S6. Relative energies in kcal/mol of the most stable intermediates for acetone hydrogenation reaction occurring on single (black) and both (grey) ruthenium sites.

XANES simulation

Ab initio XANES simulations in addition to the EXAFS fitting supported the formation of the $[\text{RuBr}_2(\text{CO})_3]_2$ complex. The detailed description of the computational routine was reported in Kozyr *et al.*⁶ Briefly, the simulation was based on the full potential finite difference method implemented in the FDMNES code,^{16, 17} and on an original approach utilizing machine learning algorithms⁵ to find the optimal 3D structure of the complex, in which all non-equivalent distances from the Ru atom to its ligands were set as variable parameters. The structure that provided the best agreement of the theoretical XANES spectrum with the experimental one (Figure S7) was characterized by Ru–Br, Ru–C, and Ru–O distances of 2.56, 1.86 and 3.03 Å, respectively. The corresponding EXAFS fit is shown in part (b) of figure S7.

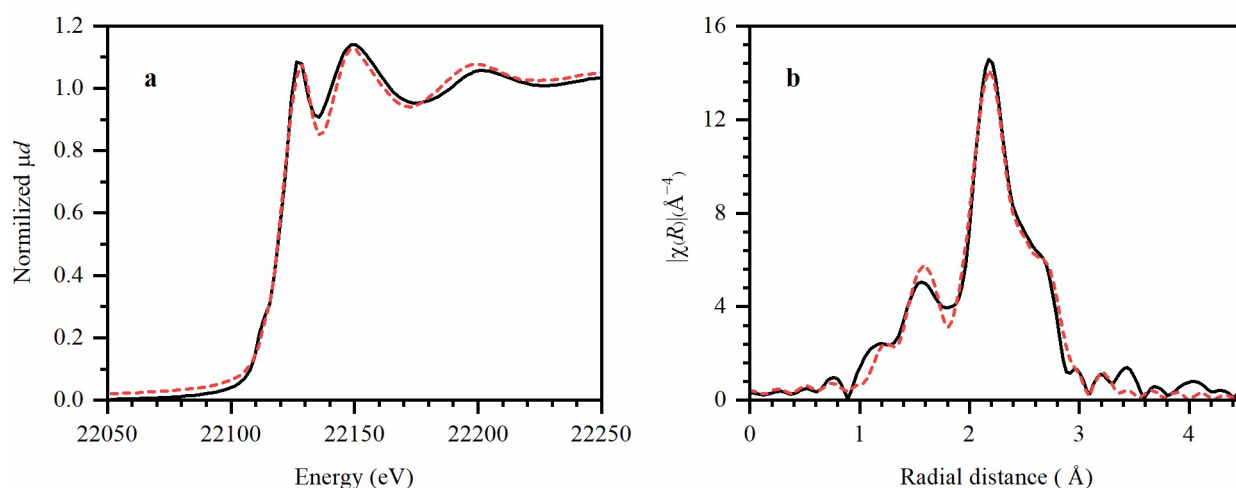


Figure S7. Experimental (solid black) and theoretical (dashed red) XANES (a) and phase-uncorrected k^3 -weighted FT-EXAFS data for $[\text{RuBr}_2(\text{CO})_3]_2$ complex.

References

1. K. Janssens, M. Stalpaert, M. Henrion and D. E. De Vos, *Chem. Commun.*, 2021, **57**, 6324-6327.
2. M. Stalpaert, K. Janssens, C. Marquez, M. Henrion, A. L. Bugaev, A. V. Soldatov and D. E. De Vos, *ACS Catal.*, 2020, **10**, 9401–9409.
3. B. Ravel and M. Newville, *J. Synchrotron Radiat.*, 2005, **12**, 537-541.
4. S. I. Zabinsky, J. J. Rehr, A. Ankudinov, R. C. Albers and M. J. Eller, *Phys. Rev. B*, 1995, **52**, 2995-3009.
5. A. Martini, S. A. Guda, A. A. Guda, G. Smolentsev, A. Algasov, O. Usoltsev, M. A. Soldatov, A. Bugaev, Y. Rusalev, C. Lamberti and A. V. Soldatov, *Comput. Phys. Commun.*, 2020, **250**, 107064.
6. E. G. Kozyr, A. L. Bugaev, S. A. Guda, A. A. Guda, K. A. Lomachenko, K. Janssens, S. Smolders, D. De Vos and A. V. Soldatov, *J. Phys. Chem. C*, 2021, **125**, 27844-27852.
7. J. Jaumot, R. Gargallo, A. de Juan and R. Tauler, *Chemom. Intell. Lab. Syst.*, 2005, **76**, 101-110.
8. R. Tauler, *Chemom. Intell. Lab. Syst.*, 1995, **30**, 133-146.
9. J. Jaumot, A. de Juan and R. Tauler, *Chemom. Intell. Lab. Syst.*, 2015, **140**, 1-12.
10. G. te Velde, F. M. Bickelhaupt, E. J. Baerends, C. Fonseca Guerra, S. J. A. van Gisbergen, J. G. Snijders and T. Ziegler, *J. Comput. Chem.*, 2001, **22**, 931-967.
11. A. D. Becke, *Phys. Rev. A*, 1988, **38**, 3098-3100.
12. S. Grimme, J. Antony, S. Ehrlich and H. Krieg, *J. Chem. Phys.*, 2010, **132**, 154104.
13. C. Lee, W. Yang and R. G. Parr, *Phys. Rev. B*, 1988, **37**, 785-789.
14. E. Van Lenthe and E. J. Baerends, *J. Comput. Chem.*, 2003, **24**, 1142-1156.
15. E. van Lenthe, A. Ehlers and E.-J. Baerends, *J. Chem. Phys.*, 1999, **110**, 8943-8953.
16. S. A. Guda, A. A. Guda, M. A. Soldatov, K. A. Lomachenko, A. L. Bugaev, C. Lamberti, W. Gawelda, C. Bressler, G. Smolentsev, A. V. Soldatov and Y. Joly, *J. Chem. Theory Comput.*, 2015, **11**, 4512-4521.
17. A. A. Guda, S. A. Guda, M. A. Soldatov, K. A. Lomachenko, A. L. Bugaev, C. Lamberti, W. Gawelda, C. Bressler, G. Smolentsev, A. V. Soldatov, Y. Joly and Iop, *J. Phys. Conf. Ser.*, 2016, **712**, 012004.